Unified modeling of total specific humidity variance in a GCM

16 décembre 2024

1 Abstract

A relevant description of atmospheric total specific humidity variance is essential in global climate models (GCM) because the performance of the cloud schemes and therefore the ability to predict cloud cover, a critical element of climate modeling uncertainties, is largely based on this variance. The aim of this work is to develop a unified prognostic model of this specific humidity variance based on turbulent transport schemes in the atmospheric column of a GCM. This prognostic model is established and implemented in the context of shallow convection to ensure consistency with previous work, but the conceptual approach and tools are designed to subsequently adapt to the mass flux scheme of deep convection with the long-term objective of making the specific humidity variance a state variable of the atmospheric model. The turbulent transport in the boundary layer is commonly modeled by the combination of a mass flux scheme of convective updrafts and a classical K-diffusive scheme. To implement the prognostic variance model, in addition to an explicit well-known formulation, we show that judicious use of the conservative formulation of tracer circulation in the mass flux routine allows variance to be transported very efficiently and elegantly. Furthermore, model adjustment is carried out using recently added automatic tuning methods which are now an integral part of the development of parameterizations.

2 Introduction

The importance of cloud representation in the radiative budget of the earth is widely documented (Bony et al., 2006; Stowasser et al., 2006; Zelinka et al., 2017) which has led climate modelers to integrate increasingly accurate cloud schemes in global climate models. Among these cloud schemes, a

classical approach consists of building a sub-grid pdf of the (total or relative) humidity or of another thermodynamic quantity such as the saturation deficit (Mellor, 1977; Sommeria and Deardorff, 1977; Jam et al., 2013) allowing us to distinguish a saturated fraction of the mesh which is associated with cloud fraction. These pdfs were gradually refined in their form, at first they were symmetrical (triangle in (Smith, 1990), rectangle in (Le Trent and Li, 1991)) but observation and LES studies has shown the importance of asymmetrical distribution especially in the convective boundary layer with cumulus clouds (Lewellen and Yoh, 1993; Larson et al., 2002). Therefore it became essential to capture this asymmetry which led to testing various pdf forms (log-normal in Bony and Emanuel (2001), beta in Tompkins (2002) or bigaussian in Jam et al. (2013),Golaz et al. (2002b)) with non-zero skewness. In parallel, the modeling of the upper moments of the distribution has also evolved, first a priori (Smith, 1990; Le Trent and Li, 1991)) then diagnosed (Bony and Emanuel, 2001; Jam et al., 2013) from thermodynamical variables or prognosed (Tompkins, 2002; Watanabe et al., 2009) from transport equations with various closure hypothesis. But whether they are established diagnostically or prognostically, it has been necessary to develop a good understanding of the physical sources of these distribution moments, in particular to close the higher-order terms related to turbulent transport.

To study the turbulent source terms of humidity variance and higher moments, the modeling of turbulent transport in GCMs is therefore a central context element. Higher-order turbulent closure models has been proposed in (Mellor and Yamada, 1982) with assumption of downgradient diffusion for the turbulent fluxes. This downgradient diffusion approach was also exploited in the context of a joint Bigaussian pdf of velocity, liquid potential temperature and total specific humidity to predict cloud cover (Golaz et al., 2002a,b; Larson et al., 2002). Though, alongside turbulent diffusion, the importance of convective structures allowing non-local countergradient transport has long been established (Deardorff (1966)). Several approaches exist to model these structures, such as for example the addition of a countergradient diffusive flux term (Lock et al. (2000)) for boundary layer turbulence, here we place ourselves within the framework of so-called mass flux schemes. Concerning the PBL, the association of these mass flux schemes, representing organized convective plumes, with a classical K-diffusion theory modeling small-scale turbulence (Mellor and Yamada (1982) Yamada (1983)), has led to the "eddy diffusion mass flux" (EDMF) models initially developed in Chatfield and Brost (1987) and widely disseminated since (Köhler et al. (2011) Hourdin et al. (2002) Rio and Hourdin (2008) Neggers et al. (2009) Pergaud J. et al. (2009)). This schemes has proven to be very effective in representing dry boundary layers with cloud formation at the tops of ascending plumes so

as stratocumulus and transition scenes (Frédéric Hourdin et al. (2019)). Mass flux schemes are also commonly used to represent deep convection scenes, in particular the Tiedke's scheme (Tiedtke (1989) and the Emanuel's scheme (Emanuel (1991)). Based on CRM studies, Klein showed the preponderant role of convective terms in explaining the evolution of the variance of total specific humidity (Klein et al. (2005)). The addition in a GCM of ad-hoc convective source terms of variance has been proposed in diagnostic (see Jam et al. (2013) for shallow convection or Bony and Emanuel (2001) for deep convection) or prognostic models (Tompkins (2002), Watanabe et al. (2009), Neggers (2009)) but the complete coupling with the mass flux model as developed by Klein does not yet seem to have been studied. In fact Klein doubted the feasibility of implementing his developments in large-scale models because of the lack of information on the variance in the thermal plume scheme. Inspired by Klein's approach and relying on an original methodology to circumvent the difficulties he raised, we propose here to integrate into a GCM the complete coupling of the mass flux scheme to the statistical cloud scheme via a prognostic variance equation. It is worth noting at this point that the choice of our Bigaussian pdf assures the closure of the third order moment of the total specific humidity given knowledge of the variance, so we don't have to develop a specific set of third order prognostic equations as in Klein et al. (2005) or Golaz et al. (2002a) for example.

In the LMDZ model, large-scale humidity variability is diagnosed from the specific humidity of ascending plumes in the mass flux schemes (shallow or deep) and from its large-scale mean value, with a bigaussian pdf in the boundary layer. Although this model is very effective for representing cumulus and stratocumulus scenes (Jam et al. (2013), Frédéric Hourdin et al. (2019), Hourdin et al. (2021), Madeleine et al. (2020)), it fails to represent some sources of variance, related to subsidence, intensity of detrainment or precipitating downdrafts for example, which can have an impact on cloud representation, especially in cases of deep convection. Rather than adding ad-hoc diagnostic terms and multiplying free parameters, we gradually moved to a global redesign of the variance model towards a prognostic approach, the first stage of which is shown here. This approach allow us to build up a unified vision of the variance evolution and its causes with very limited free paramaters. The calibration of this free paramaters in LMDZ is now achivied by using statistical learning tools based on Bayesian inference models. The principle is to use a set of 1D simulations of the model with various choices of parameters to produce a gaussian statistical emulator of some specific metrics over the hole space of parameters. These metrics are then compared to

LES simulations which makes it possible to define a subspace of satisfactory parameters.

Our main objective is therefore to establish a unified prognostic model of the large-scale variance coupled to the turbulent transport scheme in a GCM. The corresponding prognostic equations of the upper moments of specific humidity are described in (Klein et al. (2005) or Tan et al. (2018) for a more general formalism), the originality of this work lies in the methodology for implementing these equations within the framework of a GCM. Once this methodology has been established, a second objective will be to deepen the understanding of the role of the different source terms of variance linked to convection. Then we will show by the analysis of third order moments how this model, coupled with the Bigaussian cloud scheme, makes it possible to represent in a realistic way the asymmetry of the total specific humidity distribution. We focus on the implementation of this prognostic variance model in the restricted framework of shallow convection. This first step is important to lay the theoretical and methodological foundations of the new model and to compare it to the pre-existing model and to large eddy simulations (LES) in cumulus and stratocumulus scenes for which a very solid tuning strategy had been developed (Couvreux et al. (2021) Hourdin et al. (2021)). We analyse and compare cloud representation of the previous diagnostic and the new prognostic model as well as some remarkable aspects of variance and skewness especially in areas of strong detrainment. We also take the opportunity to distinguish and discuss the contributions of the different source terms of variance.

The paper is organized as follows : Section 2 presents a description of the LMDZ model setup and the methods used to develop and calibrate the new parameterization, Section 3 presents the theoretical framework in which the prognostic model takes place, in particular the elegant method which will allow us to integrate it into the convective transport scheme (method which could subsequently be extended to other transport models, diffusive or advectives for example). Section 4 documents the results obtained after tuning the free parameters of the new model, especially concerning cloud cover and specific humidity variance as well as comparisons with the previous model and discussions on the different sources of variability.

3 Model and methods

In this part, we present the LMDZ model as well as the experimental methodologies and the principle of semi-automatic tuning used to calibrate and develop the new physical parameterizations.

3.1 The LMDZ model

The parameterization which will be presented in this paper has been tested and integrated into the global climate model of Laboratoire de Météorologie Dynamique LMDZ. LMDZ is the atmospheric component of the IPSL coupled atmosphere-ocean model, IPSL-CM, used in particular for the CMIP exercises. Alongside many other physical parameterizations, the LMDZ model is characterized by a mass flux approach (Rio and Hourdin (2008)) to represent vertical turbulent transport by organized boundary layer convection. This thermal plume modele and its coupling to a bi-Gaussian cloud scheme (Jam et al. (2013)) will be presented in sections 4.2 and 4.1 as it is an essential element of the new parameterization. Deep convection on the other hand is modeled by an Emanuel's scheme in interaction with an original parameterization of cold pools created by reevaporation of convective rainfall (Grandpeix and Lafore (2010), Rio et al. (2009)).The LMDZ6A model used here, recently developed for CMIP6, includes developments in many aspects of the model Madeleine et al. (2020) as for example a modification of the thermal plume detrainment which led to a significant improvement of stratocumulus representation Hourdin et al. (2019). The LMDZ model is a flexible tool which contains in particular a single column model (SCM) version extensively used for parameterization development based on 1D/LES comparisons.

3.2 The LES cases

As described in next section 3.3 the parameterization development and calibration strategy is based on systematic comparisons of 1D cases between LES and SCM using statistical tools. Here we work specifically on cases that embrace shallow convection scenes over earth and ocean as well as stratocumulus/cumulus transitions cases. These cases were also central in the development of the thermal model in Rio and Hourdin (2008), the bi-Gaussian cloud scheme Jam et al. (2013) and the new parameterization of the thermal plume detrainment Frédéric Hourdin et al. (2019). They will be refered as IHOP/REF, ARMCU/REF, RICO/REF et SANDU/REF,FAST et SLOW and we will briefly recall the context of these different 1D cases.

IHOP comes from observations carried out during the International H_2O project on June 14, 2002 on the great plains Couvreux et al. (2005), it is an almost cloudless boundary layer.

The ARM case is derived from observations collected on 21 June 1997 at the Atmospheric Radiation Measurement site in Oklahoma, USA (Brown et al. (2002)) it represents a typical diurnal cycle of the shallow convective

boundary layer with appearance of a few cumuli clouds in the middle of the day.

The RICO case (Rain In Cumulus over the Ocean van Zanten et al. (2011)) is a case of shallow cumuli clouds over the ocean characterized by frequent precipitation.

Finally, the SANDU REF, FAST and SLOW cases are described in Sandu I. and Stevens B. (2011). They were built by compositing the large-scale conditions encountered along a set of individual Lagrangian 3-day trajectories performed for the northeastern Pacific during the summer months of 2006 and 2007. They are ment to represent oceanic boundary layers overhung by stratocumulus clouds which become thinner with a gradual transition to shallow cumulus. REF, FAST and SLOW refer to different configurations involving more or less rapid transitions.

3.3 Methodology for setting up physical parameterizations in LMDZ

As explained in Hourdin et al. (2017), the calibration of the parameterizations of a GCM is a very sensitive step in climate modeling with the multiplication of sub-grid schemes and their associated free parameters. Ideally, the calibration work should be done in successive stages from the scale of individual parameterization to the scale of the Earth's climate system as a whole, but the significant number of free parameters and parameterizations makes this work increasingly delicate. It is on this observation that automatic parameter tuning techniques were developed (Williamson et al. (2013) Williamson et al. (2015) Couvreux et al. (2021) Hourdin et al. (2021)) allowing to optimize the process and reduce biases. The principle is to rely at first on systematic 1D/LES comparisons using statistical tools so that the field of possible parameters could be reduced in successive waves. This work is then completed by an automatic 3D tuning of the global climate system compared to observations.

The intention of the tuning process is to circumscrib the space of the free parameters by comparing relevant metrics of single-column simulations of the LMDZ model with associated LES simulations. These comparisons are systematically computed using statistical tools (Williamson et al. (2013)) which explore the model parameter space in successive waves and build an emulator of the metric values. Once this emulator is built, the parameter space is reduced at each wave according to the gap between the emulated values of the metrics and the target values of the LES. This tuning process on 1D simulations not only makes it possible to significantly reduce the parameter

space but it allows us to focus and improve our understanding of the physical processes involved in the parameterizations and thus to adapt the underlying modeling work. More than a simple statistical calibration tool, it is therefore a real working support for the modeler.

Based on this approach, and using the previous mentioned 1D cases, Hourdin et al. (Hourdin et al. (2021)) were able to finely calibrate the key parameterizations on which we will step on in the present work, the thermal plume parameterization and the cloud scheme. Therefore it is essential that the new variance model proposed here is compatible with the earlier results. For this purpose we will reinvest the same tuning approach in order to obtain reliable and consistent comparison criteria with the previous work.

4 Establishment of the prognostic model of total specific humidity variance

In this part, we describe the implementation of the variance prognostic model within the physical parameterizations of LMDZ, especially the statistical cloud scheme and the thermal plume model. For this purpose it is useful to briefly recall the physical models on which these parameterizations are based.

4.1 The actual statistical cloud scheme with diagnostic variance

The LMDZ statistical cloud scheme is based on a Bigaussian pdf of saturation deficit in the presence of thermals (Jam et al. (2013)), see the descritpion of the thermal plume model in section 4.2. The saturation deficit is given by $s = a_l(q_t - q_{sat}(T_l)$ where T_l is the liquid temperature, q_t the total specific humidity, q_{sat} the total specific humidity at saturation and a_l is a factor depending on thermodynamic variables defined in Mellor (1977) Sommeria and Deardorff (1977). The Bigaussian pdf of the deficit at saturation reads :

$$pdf(s) = (1-\alpha)\mathcal{G}(s, \overline{s_{env}}, \sigma_{env}) + \alpha\mathcal{G}(s, \overline{s_{th}}, \sigma_{th}) \tag{1}$$

Where $\mathcal{G}$ is a Gaussian function of the variable s with mean value s_{env} and variance σ^2_{env} in the environment and s_{th} and σ^2_{th} inside the thermal plume, α being the fraction of the grid covered by the thermal plume. This approach is very powerfull to capture the positive skewness due to ascending plumes but we should also notice that it fails representing the negative asymmetry

due to the drying of the atmosphere by subsidence. On the other hand, subsidences are generally less organized than ascendances in local structures which reduces their impact on humidity asymemtry. With this choice of pdf using the thermal plume fraction α to fix the weights of each Gaussian term, the variance and skewness of the saturation deficit are determined by the following equations being given the standard deviations σ_{env} and σ_{th} and the mean values in both environment and thermals.

$$V = \alpha\sigma_{th}^2 + (1-\alpha)\sigma_{env}^2 + \alpha(1-\alpha)(\bar{s}_{th} - \bar{s}_{env})^2 \tag{2}$$

$$S = \frac{3\alpha(1-\alpha)(\bar{s}_{th} - \bar{s}_{env})(\sigma_{th}^2 - \sigma_{env}^2) + \alpha(1-3\alpha+2\alpha^2)(\bar{s}_{th} - \bar{s}_{env})^3}{V^{\frac{3}{2}}} \tag{3}$$

In the current diagnostic version, the standard deviations of humidity in thermals and the environment are parameterized as follows :

$$\sigma_{th} = BG2(\alpha + 0.01)^{\gamma_2}(\bar{s}_{th} - \bar{s}_{env}) + b\bar{q}_{th} \tag{4}$$

and

$$\sigma_{env} = BG1\frac{\alpha^{\gamma_1}}{1-\alpha}(\bar{s}_{th} - \bar{s}_{env}) + b\bar{q}_{env} \tag{5}$$

$BG1$, $BG2$, γ_1, γ_2 and b being tunable parameters. Once this pdf has been established, we can deduce the cloud fraction c_f of the mesh and the cloud water content q_c by :

$$c_f = \int_0^\infty pdf(s)ds \tag{6}$$

$$q_c = \int_0^\infty spdf(s)ds \tag{7}$$

4.2 The thermal plume model in LMDZ

Let ψ be a conservative variable, $\vec{v}$ the wind field and ρ the density. Using an Euler decomposition of the physical quantities $\psi = \bar{\psi} + \psi'$ and in the case of non-viscous transport, we can write :

$$\frac{\partial \bar{\psi}}{\partial t} = -\vec{v}.\vec{grad}(\bar{\psi}) - \frac{\mathrm{div}(\overline{\rho w' \psi'})}{\rho} \tag{8}$$

The first term on the right-hand is the tendency due to large-scale advection, computed by the dynamical core of the model, the second term is the tendency due to turbulent transport in which the mass flux model will intervene. In this mass flux approach, the vertical convective flux of the variable ψ is represented by :

$$\overline{\rho w' \psi'}_{th} = f(\overline{\psi_{th}} - \bar{\psi}) \tag{9}$$

where f is the convective mass flux, $\overline{\psi_{th}}$ the value of the variable in the thermal plume and $\bar{\psi}$ its value in the environment assimilated to the average value in the layer. Here the population of thermal plumes is represented by a unique thermal plume (Hourdin et al. (2002), Rio and Hourdin (2008), Rio et al. (2010), which mass flux is given by $f = \rho \alpha w_{th}$ where α is the surface fraction covered by the thermal and w_{th} the vertical speed in it. This mass flux term is added to a classic K-diffusive term $\overline{\rho w' \psi'}_{diff} = -K\rho \frac{\partial \bar{\psi}}{\partial z}$ which will be less important in this discussion.

The vertical variation of the mass flux f is given by $\frac{\partial f}{\partial z} = e - d$ where e is an entrainment term and d a detrainment term. Then we can write the vertical variation of the variable flux as :

$$\frac{\partial f \overline{\psi_{th}}}{\partial z} = e\bar{\psi} - d\overline{\psi_{th}} \tag{10}$$

Which leads to the following transport equation after some elementary algebra :

$$\frac{\partial \bar{\psi}}{\partial t} = \frac{d}{\rho}(\overline{\psi_{th}} - \bar{\psi}) + \frac{f}{\rho}\frac{\partial \bar{\psi}}{\partial z} \tag{11}$$

This formulation is the one that makes it easiest to derive the variance model. In this formulation the first term on the right-hand is the tendency due to the thermal detrainment towards the environment, the second term is the tendency associated with the compensatory subsidence in the environment the impact of which depends on the vertical gradient of the variable in the environment. Here the fact that the tendency of the variable does not depend on entrainment is linked to the assumption that the entrained air is the average air of the environment. This hypothesis simplifies both mean and variance equation.

4.3 Variance transport equation in the environment

The equation 11 cannot be directly applied to the variance of a variable because this variance is not a conservative variable. Analytical equations for the variance evolution in the presence of detraining mass fluxes has been proposed (Klein et al. (2005) with one single plume, or Tan et al. (2018) for a general formalism with N plumes) but, as pointed out before, their implementation in the climate model requires knowledge of the humidity variance in thermals. Although this is not an insurmountable difficulty in our model where it is predicted, we have chosen to implement a more straightforward, but theoretically equivalent, methodology. This approach avoids the explicit calculation of variance in thermals by separately transporting q and q^2 within the mass flux scheme. Let us first write the evolution of the variance of the total specific humidity in terms of q et q^2 :

$$\frac{\partial \overline{q'^2}}{\partial t} = \frac{\partial \overline{q^2}}{\partial t} - \frac{\partial \bar{q}^2}{\partial t} = \frac{\partial \overline{q^2}}{\partial t} - 2\bar{q}\frac{\partial \bar{q}}{\partial t} \tag{12}$$

To compute the convective variance tendency we only need knowledge of the mean total specific humidity $\bar{q}$, its convective tendency $\frac{\partial \bar{q}}{\partial t}$ and the convective tendency of the total specific humidity square $\frac{\partial \overline{q^2}}{\partial t}$. $\bar{q}$ and $\frac{\partial \bar{q}}{\partial t}$ are already calculated in the thermal plume model, therefore only $\frac{\partial \overline{q^2}}{\partial t}$ remains to be estimated. Noting that total specific humidity is a conservative variable in the thermal plume transport model, it assures that its square is also conservative (indeed, the material derivative of a squared quantity is zero if the material derivative of this quantity is zero) and can be transported with the same equation 11. At this point it may be worth to delve into the physical interpretation of the transport of q^2 as a conservative quantity.Let us begin by justifying the conservative nature of q^2, assuming that the total specific humidity q is conserve. The Lagrangian conservation of q is written as :

$$q(x + dx, y + dy, z + dz, t + dt) = q(x, y, z, t) \tag{13}$$

dx, dy, and dz being taken along the particle trajectory. Thus, for q^2, we have :

$$q^2(x + dx, y + dy, z + dz, t + dt) = q^2(x, y, z, t) \tag{14}$$

Note that the disturbance $q' = q - \bar{q}_n$ for its part cannot be considered as a conservative tracer. To convince ourselves of this, we can imagine a particle of specific humidity $q = \bar{q}_i$ (so $q' = 0$) at a level i of the model. If it is transported to another level j such that $\bar{q}_j \neq \bar{q}_i$, q' will no longer be zero in

this new layer. The disturbance q' (unlike q and q^2) cannot be interpreted as a physical quantity intrinsic to an air particle, it depends on the environment in which this particle is found and is therefore not conserved along its trajectory. With this established, the average values of q and q^2 on all the air particles at a given level n of the model and at a given time t can be written as :

$$\bar{q}_n(t) = \frac{1}{m_n} \int_{\Omega_n} q(\mathbf{x}, t) \rho d\Omega_n = \frac{1}{m_n} \sum_{p_j} q(p_j) \delta m_j \tag{15}$$

and

$$\overline{q^2}_n(t) = \frac{1}{m_n} \int_{\Omega_n} q^2(\mathbf{x}, t) \rho d\Omega_n = \frac{1}{m_n} \sum_{p_j} q^2(p_j) \delta m_j \tag{16}$$

Where m_n is the mass of the level n, Ω_n its volume, ρ the density, p_j the jth air particle of the layer and δm_j its mass. Of course it is essential to note that :

$$\frac{1}{m_n} \sum_{p_j} q^2(p_j) \delta m_j \neq (\frac{\sum_{p_j} q(p_j) \delta m_j}{m_n})^2 \tag{17}$$

The difference being the variance we are looking for. To justify our approach, we will show how the transport q as well as q^2 by the thermal model can be interpreted in terms of sums or integrals on paths of elementary fluid particles for which the Lagrangian conservation is assumed. These pathways will lead us to a formulation in the form of an exchange matrix for fluid particle transfer between the different levels of the model, using a formalism similar to that of thermal radiation exchange matrices (Cherkaoui et al. (1996), Dufresne et al. (2005)). From now on, we generalize to a conservative and intensive variable x, as are q and q^2 in the thermal model. The average value $\bar{x}_n(t)$ of this variable on all the air particles at a given level n of the model and at a given time t writes as in **??**. Now suppose that at time t, over a duration δt, a set of particles $p_{j,add}$ with total mass $m_{add} = \sum_{p_{j,add}} \delta m_{j,add}$ is added, such that $m_{add}\bar{x}_{add} = \sum_{p_{j,add}} x(p_{j,add}) \delta m_{j,add}$. The average $\bar{x}_n(t+\delta t)$ is then written as :

$$\begin{aligned} \bar{x}_n(t+\delta t) &= \frac{1}{m_n(t+\delta t)} (\sum_{p_j} x(p_j) \delta m_j + \sum_{p_{j,add}} x(p_{j,add}) \delta m_{j,add}) \\ &= \frac{1}{m_n(t+\delta t)} (m_n(t)\bar{x}_n(t) + m_{add}\bar{x}_{add}) \end{aligned} \tag{18}$$

This equation simply translates the fact that each air particle carries a certain value of x which is conserved throughout its trajectory and which is added (or subtracted on whether the particle comes or goes) in the calculation of the average $\bar{x}_n$ in proportion to its mass. Thus in these turbulent fluxes which randomly mix and redistribute the air particles, each can nevertheless be followed with the value x that it transports. This equation can be applied to both q and q^2 ; however, and this is where caution is needed, it is not valid to calculate $\bar{q}^2$. From this point on, we will no longer systematically rewrite the sums or integrals over the entire set of fluid particles. Equation 18 indeed shows that a formulation using ensemble averages accurately conveys the idea of the transport of our conservative variable by the particles. This remark is important because we do not know the individual values of x for each fluid particle. To recover the required formalism we rewrite equation 18 as :

$$\bar{x}_n(t+\delta t) = \bar{x}_n(t) + \frac{m_{add}}{m_n(t+\delta t)}(\bar{x}_{add} - \bar{x}_n(t)) \tag{19}$$

We now apply equation 19 in the context of transport of air particles by thermals with an upward mass of air carried by the plume and a subsidence in the environment.

$$\begin{aligned}\bar{x}_n(t+\delta t) = \bar{x}_n(t) &- \frac{1}{m_n(t+\delta t)} m_{n,up}(\bar{x}_{n,up} - \bar{x}_n(t)) \\ &+ \frac{1}{m_n(t+\delta t)} m_{n-1,up}(\bar{x}_{n-1,up} - \bar{x}_n(t)) \\ &+ \frac{1}{m_n(t+\delta t)} m_{n+1,down}(\bar{x}_{n+1,down} - \bar{x}_n(t)) \\ &- \frac{1}{m_n(t+\delta t)} m_{n,down}(\bar{x}_{n,down} - \bar{x}_n(t))\end{aligned} \tag{20}$$

$m_{n,up}$, $\bar{x}_{n,up}$ being the mass and mean x value of ascending particls from the thermal plume to the upper level at time t and $m_{n,down}$, $\bar{x}_{n,down}$ the descending values from the subsidence to the lower level. Considering entrainement and detrainement fluxes between the plume and the environment, mass and x conservation in the thermal plume gives as in equation 10 :

$$\begin{aligned} m_{n,up} - m_{n-1,up} &= m_e - m_d \\ m_{n,up}\bar{x}_{n,up} - m_{n-1,up}\bar{x}_{n-1,up} &= m_e\bar{x}_e - m_d\bar{x}_d \end{aligned} \tag{21}$$

m_d, $\bar{x}_d$ being the mass and mean x value of detrained particls from the plume to the environment at time t and m_e, $\bar{x}_e$ the values for the entrained particls from the environnement to the plume. Thus the equation 20 becomes :

$$\bar{x}_n(t+\delta t) = \bar{x}_n(t) + \frac{1}{m_n(t+\delta t)} m_d(\bar{x}_d - \bar{x}_n(t)) - \frac{1}{m_n(t+\delta t)} m_e(\bar{x}_e - \bar{x}_n(t))$$
$$+ \frac{1}{m_n(t+\delta t)} m_{n+1,down}(\bar{x}_{n+1,down} - \bar{x}_n(t)) - \frac{1}{m_n(t+\delta t)} m_{n,down}(\bar{x}_{n,down} - \bar{x}_n(t)) \quad (22)$$

Considering that $\bar{x}_e = \bar{x}_n(t)$, $\bar{x}_{n,down} = \bar{x}_n(t)$ and this leads to :

$$\bar{x}_n(t+\delta t) = \bar{x}_n(t) + \frac{1}{m_n(t+\delta t)} m_d(\bar{x}_d - \bar{x}_n(t)) + \frac{1}{m_n(t+\delta t)} m_{n+1,down}(\bar{x}_{n+1} - \bar{x}_n(t)) \quad (23)$$

Finally, by defining the detrainment d as the mass of air detrained per unit volume and time $d = \frac{m_d}{S\delta z \delta t}$, the entrainment $e = \frac{m_e}{S\delta z \delta t}$, and the upward flux $f = -\frac{m_{down}}{S\delta t}$, equation 23 becomes equation 11. It is therefore established that the transport equation of the thermal model conveys nothing other than the Lagrangian conservation of our variable of interest along the particle trajectories.

Now we can trace our particls back to their source through the conservation equation of x in the thermals. The discretized approach that we will develop here can be read as entirely equivalent to integral approaches using a Green's function or an adjoint transport equation (Hourdin et al. (1999) ,Hourdin and Talagrand (2006)). The goal is to highlight the influence of the different sources (here, the various levels of the model where fluid particles may come from at time $t + \delta t$).

Using the same approach than in equation 19, the stationary conservation equation 21 of variable x can be written as :

$$\hat{x}_{n+1} = \hat{x}_n + \frac{1}{\hat{m}_{n+1}} m_e(\bar{x}_e - \hat{x}_n) - \frac{1}{\hat{m}_{n+1}} m_d(\bar{x}_d - \hat{x}_n) \quad (24)$$

where $\hat{x}_n$ designs the mean value of x in the thermal plume at level n. When refering to this model as stationary, it means that the transport by the thermals occurs instantaneously at the scale of the time step δt of the large scale model. Thus, at each time step of the model, the equation 24 does not depend on δt. We now assume that $\bar{x}_d = \hat{x}_n$ and $\bar{x}_e = \bar{x}_n$. It follows that :

$$\hat{x}_{n+1} = \hat{x}_n + \frac{1}{\hat{m}_{n+1}} m_e(\bar{x}_n - \hat{x}_n) = \hat{x}_n + \frac{e_n \delta z_n}{f_n}(\bar{x}_n - \hat{x}_n) \quad (25)$$

$\hat{x}_{n+1}$ being the mean value of x in the ascending air coming up to the $(n+1)$th level. The values of $\bar{x}_n$ at the lower levels are all known and constitute the

"sources" of our problem. It is therefore possible, from this mathematical sequence, to express $\hat{x}_n$ in terms of the value $\hat{x}_{b+1} = \bar{x}_b$, which represents the entrainment at the base of the thermal, and the different values of $\bar{x}_i$ for $n > i > b$. The result will take the form $\hat{x}_n = \sum_{j=b}^{n-1} a_{j,n}\bar{x}_j$, where the $a_{j,n}$ need to be specified. It can be "easily" verified that :

$$\hat{x}_{b+2} = (1 - \frac{e_{b+1}\delta z_{b+1}}{f_{b+1}})\bar{x}_b + \frac{e_{b+1}\delta z_{b+1}}{f_{b+1}}\bar{x}_{b+1} \tag{26}$$

And for $n > (b+2)$:

$$\hat{x}_n = \prod_{j=b+1}^{n-1}(1 - \frac{e_j\delta z_j}{f_j})\bar{x}_b + \frac{e_{n-1}\delta z_{n-1}}{f_{n-1}}\bar{x}_{n-1} + \sum_{j=b+1}^{n-2}\prod_{i=j+1}^{n-1}(1 - \frac{e_i\delta z_i}{f_i})\frac{e_j\delta z_j}{f_j}\bar{x}_j \tag{27}$$

This completely defines the coefficients $a_{j,n}$ introduced above. Note that this formulation is nothing other than the vertical discretization of the integral solution of the equivalent differential equation expressed using a Green's function or the adjoint formalism. Knowing that $\bar{x}_d = \hat{x}_n$ is the detraining at level n we can substitute our coefficients into equation 23 and obtain the exchange matrix :

$$\begin{aligned}\bar{x}_n(t+\delta t) = \bar{x}_n(t)\big[1 - \frac{1}{m_n(t+\delta t)}m_d - \frac{1}{m_n(t+\delta t)}m_{n+1,down}\big] \\ + \frac{1}{m_n(t+\delta t)}m_d\sum_{j=b}^{n-1}a_{j,n}\bar{x}_j(t) + \frac{1}{m_n(t+\delta t)}m_{n+1,down}\bar{x}_{n+1}(t)\end{aligned} \tag{28}$$

$$\bar{x}_n(t+\delta t) = \sum_{i=b}^{n+1} m_{i,n}\bar{x}_i(t) \tag{29}$$

Where the coefficients $m_{i,n}$ are completely defined by the previous equation. Thus, we can express the value of $\bar{x}_n$ at time $(t+\delta t)$ as a linear function of the different sources $\bar{x}_j$ (for $b \leq j \leq n+1$) at the previous time step, which clearly illustrates the physics of transport by the thermals through the air particles that exchange between different levels. The term $(n+1)$ corresponds to the subsidence, and all terms strictly less than n are due to the ascending plume. Of course, we could continue to trace back in time step by step to reach the initial moment of the simulation, but we will not pursue the reasoning with this discretized formalism, which is quite complex to manipulate.

Two elegant and simpler formalism of analyzing the quantity of a tracer provided at a level of the model are given by the adjoint transport formalism (Hourdin et al. (1999), Hourdin and Talagrand (2006)) and the Green's

formalism. Within the framework of the adjoint formalism, Hourdin et al. (Hourdin and Talagrand (2006)) establish the equivalence between the measurement, at time t_f in a detection volume Ω_D, of the tracer of concentration q obeying the direct transport equation and the measurement, at time t_i in a source volume Ω_S, of a retrotracer of concentration q* obeying the adjoint transport equation (backtracking). Considering that at the initial instant a source distribution $\sigma = q_S\delta(t-t_i)$ ($\delta(t-t_i)$ being a temporal dirac in t_i and q_S a given concentration field) of tracer is injected into the volume Ω_S, the direct transport equation is written :

$$\frac{\partial q}{\partial t} + \vec{v}.\vec{grad}(q) = \sigma \tag{30}$$

Which is the conservation equation outside the initial time of tracer injection and whose solution can be written using a linear function $\mathcal{L}$ from the source : $q = \mathcal{L}(\sigma)$.

Similarly, if we define the measurement distribution at time t_f and over volume Ω_D as $\mu = \frac{\delta(t-tf)}{m_D(t_f)}$ (where $m_D(t_f)$ is the mass of the detection volume, please note that with these notations μ is expressed in $kg^{-1}s^{-1}$ unlike σ which is in s^{-1}), the adjoint transport equation is written :

$$-\frac{\partial q^*}{\partial t} - \vec{v}.\vec{grad}(q^*) = \mu \tag{31}$$

Whose solution can be written using a linear function $\mathcal{L}^*$ from the source : $q^* = \mathcal{L}^*(\mu)$. The retrotracer concentration is here expressed in kg^{-1}, here again note the difference in units with $\bar{q}$. With this notation the operators $\mathcal{L}$ and $\mathcal{L}^*$ are adjoint with respect to the air-mass-wheighted scalar product $<,>$ defined as :

$$< \phi, \psi >= \int_{\Omega\times\tau} \rho\phi\psi d\Omega d\tau \tag{32}$$

In this context, we can finally write :

$$< \mathcal{L}(\sigma), \mu >=< \sigma, \mathcal{L}^*(\mu) > \tag{33}$$

Which can be developped as :

$$\int_{\Omega\times\tau} \rho\mu q d\Omega d\tau = \int_{\Omega\times\tau} \rho\sigma q^* d\Omega d\tau \tag{34}$$

The left-hand side of this equation actually comes down to the integral we have already used in 15 and 16 to calculate the mean of q and q^2 at level i

of the model. In fact, the temporal dirac of the μ measurement distribution makes the temporal integration disappear and places us at time t_f. In the case of measurement of total specific humidity at time t_f at the nth level of the model, we get :

$$\int_{\Omega\times\tau} \rho\mu q d\Omega d\tau = \frac{1}{m_D} \int_{\Omega_D} q(\mathbf{x}, t_f) \rho d\Omega_D \tag{35}$$

On right-hand side of 34, taking into account the temporal Dirac of σ at t_i, we find the integral of the retrotracer concentration at the source as previously announced. This reasoning, based on the general conservation equation for q, can be extended to the case where an Eulerian decomposition $q = \bar{q} + q'$ is applied, leading to the transport equation 8 and then 11, by using the thermal model (but it could also include the diffusion model). In this case, we obtain adjoint transport equations for $\bar{q}$ and $\overline{q_{th}}$ in the thermal model. The direct and adjoint integral measures are written in the same way for $\bar{q}$:

$$\int_{\Omega\times\tau} \rho\mu\bar{q} d\Omega d\tau = \int_{\Omega\times\tau} \rho\sigma\overline{q^*} d\Omega d\tau \tag{36}$$

Note that equation 36 could be discretized over the GCM grid cells, since there is only one value for $\bar{q}$ per grid cell. Specifically, if we are interested in the measure of $\bar{q}$ over a single cell n of the model, the integral on the left-hand side of the equation then simply reduces to $\overline{q_n}$. By eliminating the time integral on the right-hand side using the Dirac delta function of the distribution σ, we then obtain :

$$\overline{q_n}(t_f) = \int_{\Omega} \rho\overline{q_S}(t_i)\overline{q^*}(t_i) d\Omega \tag{37}$$

Furthermore, it can be shown that the quantity $\int_\Omega \rho q(t)\overline{q^*}(t) d\Omega$ (q being the direct tracer and q^* the retrotracer) is conserved over time.

We now turn our attention to Green's formalism, which will provide a complementary perspective to the analyses above. The system of transport equations 10 and 11 for $\bar{q}$ and $\overline{q_{th}}$ is a linear system whose solution can be expressed using the Green's propagator functions, denoted as $g(\mathbf{x}, t|\mathbf{x_S}, t_i)$, given the initial conditions q_S. For a cell n of the model, this solution is expressed as :

$$\overline{q_n}(t_f) = \int_{\Omega} \rho g(\mathbf{x_n}, t_f|\mathbf{x_S}, t_i)\overline{q_S}(t_S) d\Omega \tag{38}$$

The Green's function is naturally interpreted as the propagation function of sources to the point and time of observation. This clearly shows the convergence between the two formalisms : by comparing equations 38 and 37, the

Green's function, which is the direct response of the problem at $(\mathbf{x_n}, t_f)$, corresponds to the response of the adjoint problem at $(\mathbf{x_S}, t_S)$. This is a well-known property of the direct and adjoint Green's functions of a linear system. Note that the use of this formalism allows for the development of backtracking Monte Carlo methods, which can be advantageously coupled with the climate model (see Tregan et al. (2023),Villefranque et al. (2022) for further details).

After these theoretical considerations, we are now justified in transporting the square of the total specific humidity as a conservative tracer, just like the total specific humidity itself. So to compute equation 12 we only have to call the plume transport routine for both total humidity and its square, instead of just the first one, with no need to implement further equations. Of course we can check the consistency of this approach by deriving the analytical development which joins and provides another perspective on the Klein's formalism of variance transport. Applying the equation 11 both to q and q^2, we obtain :

$$\frac{\partial \overline{q'^2}}{\partial t} = \frac{d}{\rho}(\overline{q_{th}^2} - \overline{q^2}) + \frac{f}{\rho}\frac{\partial \overline{q^2}}{\partial z} - 2\bar{q}[\frac{d}{\rho}(\overline{q_{th}} - \bar{q}) + \frac{f}{\rho}\frac{\partial \bar{q}}{\partial z}] \tag{39}$$

Subsidence terms combine as follows : $\frac{f}{\rho}\frac{\partial \overline{q^2}}{\partial z} - 2\bar{q}\frac{f}{\rho}\frac{\partial \bar{q}}{\partial z} = \frac{f}{\rho}\frac{\partial \overline{q'^2}}{\partial z}$. Detrainment terms can also be rearranged : $(\overline{q_{th}^2} - \overline{q^2}) - 2\bar{q}(\overline{q_{th}} - \bar{q}) = (\overline{q_{th}} - \bar{q})^2 + (\overline{q_{th}'^2} - \overline{q'^2})$. And the convective variance tendency finally reads :

$$\frac{\partial \overline{q'^2}}{\partial t} = \frac{d}{\rho}[(\overline{q_{th}} - \bar{q})^2 + (\overline{q_{th}'^2} - \overline{q'^2})] + \frac{f}{\rho}\frac{\partial \overline{q'^2}}{\partial z} \tag{40}$$

This approach leads to a similar equation that Klein (Klein et al. (2005)) derives from the mixing of two air masses and its impact on the humidity variance in the environment. This is not surprising because both approaches ultimately relie on the air mass conservation equations. In the present formalism we can underline the absence of the entrainment term, due to the already mentioned fact that we assumed that the entrained air had the average composition of the environment. We can interpret the different terms of the equation 40 as follows :

- The first represents the impact of the mean values difference between the thermal plume and the environment
- The second expresses the impact of the variances difference between the thermal plume and the environment
- The last one expresses, due to compensatory subsidence, highlights the role of the vertical gradient of variance

Note that this variance transport equation is limited to organized convective sources which are supposed to be dominant in the studied cases, it could subsequently include the diffusive terms, computed with the same approach by calling the diffusive transport model for both q and q^2. We could also include possible source/sink terms due to evaporation of precipitation for instance, or large-scale advection, this will be the subject of forthcoming publication. Here we place ourselves in a framework where the transport of variance is carried out by the organized convective terms and we only add a classical exponential dissipation term representing the small scale homogenization processes which will be discussed in the next section 4.4. The present model finally reads :

$$\frac{\partial \overline{q'^2}}{\partial t} = \frac{d}{\rho}[(\overline{q_{th}} - \bar{q})^2 + (\overline{q_{th}^2} - \overline{q'^2})] + \frac{f}{\rho}\frac{\partial \overline{q'^2}}{\partial z} - \frac{\overline{q'^2}}{\tau} \tag{41}$$

where τ represents the relaxation time of the variance in the environment. In practice we can either implement this variance equation term by term or call the thermal transport equation for q and q^2 as described before. However, the two methods lead to very different implementation of the variance model, each of which having its own interest. In the first method we explicitly calculate the different terms of the equation 41 which allows us to compare the relative importance of this terms, especially the one associated to the difference in humidity mean and variance. The second way is much simpler to implement and can be transposed to other transport processes (diffusive transport or large-scale advection for example). In this case it is no longer necessary to extract all the physical quantities from the thermal model, only the tendencies of $\overline{q^2}$ and $\bar{q}$ are necessary. The two ways of proceeding are completely equivalent, the first allows better analysis of the physical content of the model, the second has the advantage of very great simplicity of implementation and provides a methodology that can easily be transposed to other models.

4.4 The relaxation time in the variance model

The Newton relaxation time τ which appears in the dissipation term is an important parameter of the variance calculation. It can be estimated by assimilation to the relaxation time of the turbulent energy as was proposed in Nieuwstadt and Brost (1986) Neggers (2009). Tompkins (Tompkins (2002) proposes to divide this relaxation time into two components : a first one based on quite fast small-scale 3D turbulence as before, and a second one

representing very slower large-scale two-dimensional dissipation due to horizontal wind shear instability. This second component would be present even in case of strong temperature stratification. Although it will be a part of our reflection when it comes to the upper atmosphere, we neglect it here, as we only focus on shallow convective cases where the first component is totally dominant. The order of magnitude of the turbulence depending relaxation time is given by :

$$\tau = \frac{l}{w*} \tag{42}$$

where $w* = \sqrt{TKE}$ (TKE being the turbulent kinetic energy) is a typical vertical speed associated with turbulent phenomena, l a mixing length of roughly 100m (Blackadar (1962)). We obtain an order of magnitude of 100s to 1000s for τ which is a fairly fast relaxation, especially compared to the 10-days estimated 2D relaxation (Tompkins (2002)). The adjustment of the parameter τ is the only tuning issue of the present model. It has been performed in two manners : first as an entirely free parameter, then by using equation 42 with a free multiplicative factor. Let us specify that in this second case, it was necessary, as in Golaz et al. (2002a), to define an upper limit to relaxation time as our TKE is likely to cancel out even below 3000m. This prevents the relaxation terms from becoming too small and allowing the variance to accumulate too strongly.

4.5 Injecting the total specific humidity variance into the cloud scheme

To replace the previous diagnostic model with a prognostic model based on humidity variance transport equations, it is first necessary to connect the humidity variance to the variance of the saturation deficit which drives the statistical cloud scheme. This well-known relationship (Tompkins (2002)) can be written as :

$$\sigma(s)^2 = a_l^2(\overline{q'^2} + \alpha_l^2\overline{T_l'^2} - 2\alpha_l\overline{q'}\overline{T_l'}) \tag{43}$$

Where $\alpha_l = (\frac{\partial q_{sat}}{\partial T})_{T_l}$, a_l was mentioned in section 4.1 and T_l is the liquid temperature.

We see that a liquid temperature variance term appears in this equation as well as a cross-correlation term whose physical interpretations are described in Tompkins (2003) for example. Several studies have analyzed the relative importance of humidity and temperature contributions to variance

(Price (2001) Tompkins (2003)). Although the temperature contribution is not completely negligible, it appears from these analyzes that order 1 is mostly dominated by the variability of specific humidity. In the context of this work, it seemed relevant to mainly concentrate on the specific humidity variability. Orders of magnitude of these variabilities can be estimated in LMDZ by simply diagnosing the differences in humidity and liquid temperature between the thermals and the environment, on this basis we obtain an order of magnitude of $10^{-4}kg/kg$ for $\overline{q'^2}$ and closer to $10^{-5}kg/kg$ for $\alpha_l^2\overline{T_l'^2}$. In this work the hypothesis will be made that the variance of s is controlled by the variance of the total specific humidity. Therefore the humidity variance computed by the prognostic model will be injected into σ_{env} (after multiplication by a_l) instead of being prescribed by the diagnostic parameterization.

5 Results

5.1 Tuning setup

In this part, we resume the 1D tuning work carried out on the IHOP, ARMCU, RICO and SANDU cases in Couvreux et al. (2021) Hourdin et al. (2021) by adding the variance model and its relaxation time as a free parameter. We use the same metrics as in paragraph 5.1 of Hourdin et al. (2021) to compare SCM simulations to LES. The free parameters are also the same with exchanging the diagnostic model parameter $BG1$ by the parameter τ, allowed to vary between 100s and 2000s.

We briefly recall the choice of metrics for the tuning process, for more details on the mathematical formalisms, refer to Hourdin et al. (2021). The metrics used to compare 1D GCM simulations to LES are based on three quantities : potential temperature, humidity and cloud cover. These metrics are defined by temporal and spatial integrations of the three quantities over time and altitudes. For cloud cover, three specific metrics are used, the first is linked to the maximum cloud cover on the vertical $\alpha_{cld,max}$, the second represents an average altitude of the cloud cover $z_{cld,ave}$ and the last one tells us about the typical altitude of the maximum cloud cover $z_{cld,max}$. Figure 1 details all the differnet metrics used in this tuning (the three cloud metrics, and those concerning potential temperature and humidity).

Concerning the free parameters to be tuned, our description will also be quite brief, please refer again to Hourdin et al. (2021) for the formal details. These parameters primarily concern the modeling of the entrainment and detraining rate of the thermal plume model which depend on the buoyancy and the vertical speed in the ascent (these parameterizations are controlled

Case Subcase	IHOP REF	ARMCU REF	RICO REF	SANDU REF	SANDU SLOW	SANDU FAST
time	7-9	7-9	19-25	50-60	50-60	50-60
$\theta_{400-600m}$	×	×	×			
$q_{v,400-600m}$		×				
$\alpha_{cld,max}$		×	×			
$z_{cld,ave}$		×		×		
$z_{cld,max}$		×		×	×	×

FIGURE 1 – Metrics for the 1D/LES tuning. Time average is given in hours from the beginning of the simulation. Potential temperature is given in K, humidity in kg/kg and heights in m.

by the parameters $A1$, $B1$, $B2$, CQ). The modification of the detraining rate proposed in Frédéric Hourdin et al. (2019) introduces a characteristic height difference in the calculation of buoyancy which is controlled by the DZ parameter. The $BG2$ parameter (see paragraph 4.1) is linked to the standard deviation of humidity in the thermal plume. The parameter $BG1$ of the diagnostic variance model, see section 4.1, was removed and logically replaced by the relaxation time of the new model. Finally, the CLC and EVAP parameters are involved in the precipitation and rain re-evaporation model, CLC being associated with the critical incloud water from which precipitation is activated and EVAP being a free parameter of the precipitation flux equation which controls the fraction of precipitation that re-evaporates at a given altitude. The formalism of these parameterizations was introduced by the work of Sundqvist in Sundqvist (1978). Figure 2 presents a summary of the different parameters to be tuned.

5.2 Simulation scores according to the tuning tool

At each tuning wave, LMDZ SCM-simulations are computed within the range of authorized parameters by the previous wave (NROY : not-ruled out yet). For each of this simulations, a score is assigned per metric, this score being defined from the difference between the target value of the metric (the average value of the LES) and the value for the given simulation, as well as from the accepted tolerance. The closer the score is to 0, the closer the simulation metric is to the target value, a score equal to 1 indicates that the difference between the simulated metric and the target value corresponds

Name	Min	Max	Ref	Sampling	controls
A1	0.5	1.2	2.	linear	contribution of buyoncy to the plume acceleration
A2	$1.5e-3$	$4.e-3$	$2.e-3$	linear	drag term in the plume acceleration
B1	0.	1.	0.95	linear	scaling factor for entrainment and detrainment
CQ	0.	0.02	0.012	linear	influence of humidity contrast on detrainment
DZ	0.05	0.2	0.07	linear	environmental air altitude shift for buyoncy computation
BG2	0.03	0.2	0.09	linear	width of the plume subgrid scale water distribution
EVAP	$5.e-5$	$5.e-4$	$1.e-4$	log	reevaporation of rainfall
CLC	$1.e-4$	$1.e-3$	$6.5e-4$	linear	autoconversion of cloud liquid water to rainfall
tau_var	100.	2000	700	linear	timescale for variance dissipation

FIGURE 2 – Free parameters of the 1D/LES tuning

exactly to the tolerance which we are willing to accept. The simulations can thus be classified according to the obtained scores, either on an average score criterion or on a maximum criterion. Her we use the maximum criterion to classify the ten most efficient simulations in order to prevent large errors on certain metrics from being compensated by very good results on others.

Figure 3 compares the results obtained on all the metrics between the diagnostic and prognostic models. In particular we see that the ten best simulations achieve almost identical scores in both cases, close or even lower than 1. The distribution of scores in the different metrics is also very similar. In particular, one of the key points which limits the performance of the model is the difficulty in jointly representing the maximum cloud cover of the RICO and ARMCU cases : the first being too big and the second too small.

It is important to underline that the tuning process does not aim to select an optimized configuration of the model but rather to highlight a range of parameters leading to acceptable results within the framework we have defined and the typical performance of the model in this range. In this context this tuning showed that the acceptable range of the relaxation time is 300s to 800s which is consistent with the previous qualitative considerations. Or, if using the TKE to define the relaxation time, the acceptable range of the mixing lenght shows up to be 70m to 160m.

5.3 Comparisons of variances and cloud covers

In this section, we focus on the variance and cloud covers profiles which are the main observables of this work, being noticed that most physical quantities are little affected by the change in variance parameterization as observed in section 5.2. Figure 4 plots the vertical profiles of humidity variance in ARMCU/REF, RICO/REF and SANDU/REF and its evolution over time, comparison is made between the old diagnostic model, the new prognostic model and the LES. Figure 7 plots the vertical profiles of cloud cover over time in the three studied cases and compares the results of the diagnostic and prognostic model both facing the LES.

Here again we see a very strong similarity between the two models, both very close to the LES simulation. One of the recently resolved default of the LMDZ cloud scheme was to reproduce a fairly satisfying cloud profiles of stratocumulus and stratocumulus to cumulus transition cases (Hourdin et al. (2019)) with their almost total cloud cover. Hourdin et al. show how a judicious modification of the detrainment parameterization made it possible to correct this problem. Therefore it is interesting to focus on the SANDU transition case. Despite the qualitative leap allowed by the new parameterization of the detrainment established in Frédéric Hourdin et al. (2019), we see that the cloud cover tends to remain saturated while it gradually fades in the LES. Moreover this cloud cover is a little too thick at night in LMDZ especially from of the second day of the simulation where it becomes significantly finer in the LES. Figures 7 and 4 shows that these two aspects are attenuated with the new variance prognostic model. Looking deeper at the variance profile, we can attribute this improvement to a better representation of the variance peak at the top of the clouds. Let's remind, indeed, that an increase in the variance of the statistical cloud scheme, in case of high cloud cover, is likely to reduce the cloud cover by increasing the fraction of air with lower humidity. This better representation of the variance peak can partly be attributed to the thermal plume detrainment peak in this area as we can see in Figure 5 (in the middle bottom) even if this peak seems to take place a little too high. In fact, the detrainment is directly involved in the variance transport equation but it cannot be captured by the old diagnostic model which does not take it into account but only contains a multiplicative term depending on the thermal fraction (dashed red curve in the middle of Figure 5). This term vanishes to zero while the detrainment reaches its peak which explains the difference in behavior between the two models. We can notice, however, that the great difference in humidity between thermals and environment plays a crucial role at these altitudes (in green in Figure 5 in the middle) but in the diagnostic model this term is multiplied by a factor

which tends quickly to zero while in the prognostic model the multiplicative factor, which depends on the detrainment, cancels out later and can even reach a local maximum at the top of the clouds.

Another interesting information from this study is the clear predominance of the first term of the variance transport equation 40 (see Figure 5 on the left), a term which represents the squared difference in humidity between thermals and environment. Difference of variance and subsidence terms appear to be an order of magnitude smaller so that it could be neglected if we want to simplify the implementation of the explicit transport equation in the model. This will be very usefull when it comes to deep convection transport, which will be treated in a future publication, and more generally in cases where the model does not predict the humidity variance in the updraft but only its mean humidity. Let us specify that this dominance of the first term doesn't match Klein's study Klein et al. (2005) where the first two terms are of the same order of magnitude, the last one being smaller.

Finally we can also focus on the profiles of the third order moments of the saturation deficit distribution (Figure 6). At first, while the predictions of the new prognostic model (in blue) are globally realistic, we notice a little tendency to overestimate the skewness (or the centered third order moment). A possible explanation, already mentioned before, is the lack of representation in the pdf of organized subsidizing structures which tend to locally dry out the environment. Although subsidences are taken into account as sources of variance, they cannot negatively impact the third order moment because of the binary structure of our pdf with only thermal plume and environment. This is particularly visible in rare areas of negative skewness but it should not overshadow the quite accurate estimation of the third-order moments of the model.

Concerning the previous diagnostic model (dashed red curve), there is an inconsistent drift in the skewness at the cloud tops, but a more detailed analysis shows that this drift is entirely explained by the premature cancellation of the variance, as we mentioned earlier. Indeed, the third-order centered moment, when not normalized by the variance, behaves very similar to the prognostic model.

This shows that the choice of a weighted bivariate Gaussian pdf, based on the fraction of thermals, provides a satisfactory framework for representing the asymmetric distribution of humidity at different atmospheric levels especially when associated with the prognostic variance model, which helps avoid inconsistent behaviors at the cloud tops through the thermal detrainment term.

6 conclusion

In the work presented above, we focused on designing and testing in a GCM a prognostic model of the variance of total specific humidity whose physical content is based on the general transport equations. In the context of shallow convection, we made large use of the thermal plume model in which the specific humidity is treated as a conservative variable. This property allowed us to easily transport its square and show off the equation of evolution of the variance by assimilating the diffusive homogenization to a simple Newtonian relaxation revealing a time parameter which can be estimated from the tke. The implementation of this model coupled to a Bigaussian statistical cloud scheme made it possible to reproduce with great consistency the previous results obtained with the diagnostic model by using new automatic tuning tools. In particular, the vertical variance and cloud cover profiles are close to LES in the shallow convection and transition cases ARMCU, RICO, SANDU, and IHOP. Certain defective characteristics of these profiles could be erased with the new model, in particular at the top of the clouds where a peak of detrainment can have a significant impact on the variance and skewness. As a natural extension of this work, and it is in progress, it will be relevant to integrate the formalism of the Emanuel's scheme for deep convection into the variance model and further source terms like evaporation. A last step would be to transport the large-scale variance as a state variable in the dynamics of the model with the same approach, that is to say by calling the transport of the specific humidity square to compute the variance tendency.

Références

Blackadar, A. K., 1962 : The vertical distribution of wind and turbulent exchange in a neutral atmosphere, *Journal of Geophysical Research (1896-1977)*, **67**, 3095–3102, _eprint : https ://onlinelibrary.wiley.com/doi/pdf/10.1029/JZ067i008p03095.

Bony, S., and K. A. Emanuel, 2001 : A Parameterization of the Cloudiness Associated with Cumulus Convection ; Evaluation Using TOGA COARE Data, *Journal of the Atmospheric Sciences*, **58**, 3158–3183.

Bony, S., R. Colman, V. M. Kattsov, R. P. Allan, C. S. Bretherton, J.-L. Dufresne, A. Hall, S. Hallegatte, M. M. Holland, W. Ingram, D. A. Randall, B. J. Soden, G. Tselioudis, and M. J. Webb, 2006 : How Well Do We Understand and Evaluate Climate Change Feedback Processes ?,

Journal of Climate, **19**, 3445–3482, publisher : American Meteorological Society Section : Journal of Climate.

Brown, A. R., R. T. Cederwall, A. Chlond, P. G. Duynkerke, J.-C. Golaz, M. Khairoutdinov, D. C. Lewellen, A. P. Lock, M. K. MacVean, C.-H. Moeng, R. A. J. Neggers, A. P. Siebesma, and B. Stevens, 2002 : Large-eddy simulation of the diurnal cycle of shallow cumulus convection over land, *Quarterly Journal of the Royal Meteorological Society*, **128**, 1075–1093.

Chatfield, R. B., and R. A. Brost, 1987 : A two-stream model of the vertical transport of trace species in the convective boundary layer, *Journal of Geophysical Research : Atmospheres*, **92**, 13263–13276, _eprint : https ://onlinelibrary.wiley.com/doi/pdf/10.1029/JD092iD11p13263.

Cherkaoui, M., J.-L. Dufresne, R. Fournier, J.-Y. Grandpeix, and A. Lahellec, 1996 : Monte Carlo Simulation of Radiation in Gases With a Narrow-Band Model and a Net-Exchange Formulation, *Journal of Heat Transfer*, **118**, 401–407.

Couvreux, F., F. Guichard, J. L. Redelsperger, C. Kiemle, V. Masson, J. P. Lafore, and C. Flamant, 2005 : Water-vapour variability within a convective boundary-layer assessed by large-eddy simulations and IHOP_2002 observations, *Quarterly Journal of the Royal Meteorological Society*, **131**, 2665–2693, aDS Bibcode : 2005QJRMS.131.2665C.

Couvreux, F., F. Hourdin, D. Williamson, R. Roehrig, V. Volodina, N. Villefranque, C. Rio, O. Audouin, J. Salter, E. Bazile, F. Brient, F. Favot, R. Honnert, M.-P. Lefebvre, J.-B. Madeleine, Q. Rodier, and W. Xu, 2021 : Process-Based Climate Model Development Harnessing Machine Learning : I. A Calibration Tool for Parameterization Improvement, *Journal of advances in modeling earth systems*, **13**, n/a–n/a.

Deardorff, J. W., 1966 : The Counter-Gradient Heat Flux in the Lower Atmosphere and in the Laboratory, *Journal of the Atmospheric Sciences*, **23**, 503–506, publisher : American Meteorological Society Section : Journal of the Atmospheric Sciences.

Dufresne, J.-L., R. Fournier, C. Hourdin, and F. Hourdin, 2005 : Net Exchange Reformulation of Radiative Transfer in the CO2 15-μm Band on Mars, *Journal of the Atmospheric Sciences*, **62**, 3303–3319, publisher : American Meteorological Society Section : Journal of the Atmospheric Sciences.

Emanuel, K. A., 1991 : A Scheme for Representing Cumulus Convection in Large-Scale Models, *Journal of the Atmospheric Sciences*, **48**, 2313–2329, publisher : American Meteorological Society Section : Journal of the Atmospheric Sciences.

Frédéric Hourdin, Arnaud Jam, Catherine Rio, Fleur Couvreux, Irina Sandu, Marie-Pierre Lefebvre, Florent Brient, and Abderrahmane Idelkadi, 2019 : Unified Parameterization of Convective Boundary Layer Transport and Clouds With the Thermal Plume Model, **11**, 2910–2933.

Golaz, J.-C., V. E. Larson, and W. R. Cotton, 2002*a* : A PDF-Based Model for Boundary Layer Clouds. Part I : Method and Model Description, *Journal of the Atmospheric Sciences*, **59**, 3540–3551, publisher : American Meteorological Society Section : Journal of the Atmospheric Sciences.

Golaz, J.-C., V. E. Larson, and W. R. Cotton, 2002*b* : A PDF-Based Model for Boundary Layer Clouds. Part II : Model Results, *Journal of the Atmospheric Sciences*, **59**, 3552–3571, publisher : American Meteorological Society Section : Journal of the Atmospheric Sciences.

Grandpeix, J.-Y., and J.-P. Lafore, 2010 : A Density Current Parameterization Coupled with Emanuel's Convection Scheme. Part I : The Models, *Journal of the Atmospheric Sciences*, **67**, 881–897, publisher : American Meteorological Society Section : Journal of the Atmospheric Sciences.

Hourdin, F., and O. Talagrand, 2006 : Eulerian backtracking of atmospheric tracers. I : Adjoint derivation and parametrization of subgrid-scale transport, *Quarterly Journal of the Royal Meteorological Society*, **132**, 567–583, _eprint : https ://onlinelibrary.wiley.com/doi/pdf/10.1256/qj.03.198.A.

Hourdin, F., J.-P. Issartel, B. Cabrit, and A. Idelkadi, 1999 : Reciprocity of atmospheric transport of trace species, *Comptes Rendus de l'Académie des Sciences - Series IIA - Earth and Planetary Science*, **329**, 623–628.

Hourdin, F., F. Couvreux, and L. Menut, 2002 : Parameterization of the Dry Convective Boundary Layer Based on a Mass Flux Representation of Thermals, *Journal of the Atmospheric Sciences*, **59**, 1105–1123.

Hourdin, F., T. Mauritsen, A. Gettelman, J.-C. Golaz, V. Balaji, Q. Duan, D. Folini, D. Ji, D. Klocke, Y. Qian, F. Rauser, C. Rio, L. Tomassini, M. Watanabe, and D. Williamson, 2017 : The Art and Science of Climate Model Tuning, *Bulletin of the American Meteorological Society*, **98**, 589–602, publisher : American Meteorological Society Section : Bulletin of the American Meteorological Society.

Hourdin, F., A. Jam, C. Rio, F. Couvreux, I. Sandu, M.-P. Lefebvre, F. Brient, and A. Idelkadi, 2019 : Unified Parameterization of Convective Boundary Layer Transport and Clouds With the Thermal Plume Model, *Journal of Advances in Modeling Earth Systems*, **11**, 2910–2933.

Hourdin, F., D. Williamson, C. Rio, F. Couvreux, R. Roehrig, N. Villefranque, I. Musat, L. Fairhead, F. B. Diallo, and V. Volodina, 2021 : Process-Based Climate Model Development Harnessing Machine Learning : II. Model Calibration From Single Column to Global, *Journal of advances in modeling earth systems*, **13**, n/a–n/a.

Jam, A., F. Hourdin, C. Rio, and F. Couvreux, 2013 : Resolved Versus Parametrized Boundary-Layer Plumes. Part III : Derivation of a Statistical Scheme for Cumulus Clouds, *Boundary-Layer Meteorology : An International Journal of Physical, Chemical and Biological Processes in the Atmospheric Boundary Layer*, **147**, 421–441.

Klein, S. A., R. Pincus, C. Hannay, and K.-M. Xu, 2005 : How might a statistical cloud scheme be coupled to a mass-flux convection scheme ?, *Journal of Geophysical Research : Atmospheres*, **110**.

Köhler, M., M. Ahlgrimm, and A. Beljaars, 2011 : Unified treatment of dry convective and stratocumulus-topped boundary layer in the ECMWF model, *Quarterly Journal of the Royal Meteorological Society*, **137**, 43–57.

Larson, V. E., J.-C. Golaz, and W. R. Cotton, 2002 : Small-Scale and Mesoscale Variability in Cloudy Boundary Layers : Joint Probability Density Functions, *Journal of the Atmospheric Sciences*, **59**, 3519–3539, publisher : American Meteorological Society Section : Journal of the Atmospheric Sciences.

Le Trent, H., and Z.-X. Li, 1991 : Sensitivity of an atmospheric general circulation model to prescribed SST changes : feedback effects associated with the simulation of cloud optical properties, *Climate Dynamics*, **5**, 175–187.

Lewellen, W. S., and S. Yoh, 1993 : Binormal Model of Ensemble Partial Cloudiness, *Journal of the Atmospheric Sciences*, **50**, 1228–1237, publisher : American Meteorological Society Section : Journal of the Atmospheric Sciences.

Lock, A. P., A. R. Brown, M. R. Bush, G. M. Martin, and R. N. B. Smith, 2000 : A New Boundary Layer Mixing Scheme. Part I : Scheme Descrip-

tion and Single-Column Model Tests, *Monthly Weather Review*, **128**, 3187–3199, publisher : American Meteorological Society Section : Monthly Weather Review.

Madeleine, J.-B., F. Hourdin, J.-Y. Grandpeix, C. Rio, J.-L. Dufresne, E. Vignon, O. Boucher, D. Konsta, F. Cheruy, I. Musat, A. Idelkadi, L. Fairhead, E. Millour, M.-P. Lefebvre, L. Mellul, N. Rochetin, F. Lemonnier, L. Touzé-Peiffer, and M. Bonazzola, 2020 : Improved Representation of Clouds in the Atmospheric Component LMDZ6A of the IPSL-CM6A Earth System Model, *Journal of advances in modeling earth systems*, **12**, n/a–n/a.

Mellor, G. L., and T. Yamada, 1982 : Development of a turbulence closure model for geophysical fluid problems, *Reviews of Geophysics*, **20**, 851–875, _eprint : https ://onlinelibrary.wiley.com/doi/pdf/10.1029/RG020i004p00851.

Mellor, G. L., 1977 : The Gaussian Cloud Model Relations, *Journal of the Atmospheric Sciences*, **34**, 356–358, publisher : American Meteorological Society Section : Journal of the Atmospheric Sciences.

Neggers, R., M. Kohler, and A. Beljaars, 2009 : A Dual Mass Flux Framework for Boundary Layer Convection. Part I : Transport, *JOURNAL OF THE ATMOSPHERIC SCIENCES*, **66**, 1465–1487.

Neggers, R., 2009 : A Dual Mass Flux Framework for Boundary Layer Convection. Part II : Clouds, *JOURNAL OF THE ATMOSPHERIC SCIENCES*, **66**, 1489–1506.

Nieuwstadt, F. T. M., and R. A. Brost, 1986 : The Decay of Convective Turbulence, *Journal of the Atmospheric Sciences*, **43**, 532–546, publisher : American Meteorological Society Section : Journal of the Atmospheric Sciences.

Pergaud J., Masson V., Malardel S., and Couvreux F., 2009 : A parameterization of dry thermals and shallow cumuli for mesoscale numerical weather prediction, *Boundary-Layer Meteorology*, **132**, 83–106.

Price, J. D., 2001 : A study of probability distributions of boundary-layer humidity and associated errors in parametrized cloud-fraction, *Quarterly Journal of the Royal Meteorological Society*, **127**, 739–758, _eprint : https ://onlinelibrary.wiley.com/doi/pdf/10.1002/qj.49712757302.

Rio, C., and F. Hourdin, 2008 : A Thermal Plume Model for the Convective Boundary Layer : Representation of Cumulus Clouds, *Journal of the Atmospheric Sciences*, **65**, 407–425.

Rio, C., F. Hourdin, J.-Y. Grandpeix, and J.-P. Lafore, 2009 : Shifting the diurnal cycle of parameterized deep convection over land, *Geophysical Research Letters*, **36**, _eprint : https ://onlinelibrary.wiley.com/doi/pdf/10.1029/2008GL036779.

Rio, C., F. Hourdin, F. Couvreux, and A. Jam, 2010 : Resolved Versus Parametrized Boundary-Layer Plumes. Part II : Continuous Formulations of Mixing Rates for Mass-Flux Schemes, *Boundary-Layer Meteorology*, **135**, 469–483, aDS Bibcode : 2010BoLMe.135..469R.

Sandu I., and Stevens B., 2011 : On the factors modulating the stratocumulus to cumulus transitions, *Journal of the Atmospheric Sciences*, **68**, 1865–1881.

Smith, R. N. B., 1990 : A scheme for predicting layer clouds and their water content in a general circulation model, *Quarterly Journal of the Royal Meteorological Society*, **116**, 435–460.

Sommeria, G., and J. W. Deardorff, 1977 : Subgrid-Scale Condensation in Models of Nonprecipitating Clouds, *Journal of the Atmospheric Sciences*, **34**, 344–355, publisher : American Meteorological Society Section : Journal of the Atmospheric Sciences.

Stowasser, M., K. Hamilton, and G. J. Boer, 2006 : Local and Global Climate Feedbacks in Models with Differing Climate Sensitivities, *Journal of Climate*, **19**, 193–209.

Sundqvist, H., 1978 : A parameterization scheme for non-convective condensation including prediction of cloud water content, *Quarterly Journal of the Royal Meteorological Society*, **104**, 677–690.

Tan, Z., C. M. Kaul, K. G. Pressel, Y. Cohen, T. Schneider, and J. Teixeira, 2018 : An Extended Eddy-Diffusivity Mass-Flux Scheme for Unified Representation of Subgrid-Scale Turbulence and Convection, *Journal of Advances in Modeling Earth Systems*, **10**, 770–800, _eprint : https ://onlinelibrary.wiley.com/doi/pdf/10.1002/2017MS001162.

Tiedtke, M., 1989 : A Comprehensive Mass Flux Scheme for Cumulus Parameterization in Large-Scale Models, *Monthly Weather Review*, **117**, 1779–1800, publisher : American Meteorological Society Section : Monthly Weather Review.

Tompkins, A. M., 2002 : A Prognostic Parameterization for the Subgrid-Scale Variability of Water Vapor and Clouds in Large-Scale Models and Its Use to Diagnose Cloud Cover, *Journal of the Atmospheric Sciences*, **59**, 1917–1942.

Tompkins, A. M., 2003 : Impact of temperature and humidity variability on cloud cover assessed using aircraft data, *Quarterly Journal of the Royal Meteorological Society*, **129**, 2151–2170, _eprint : https ://online-library.wiley.com/doi/pdf/10.1256/qj.02.190.

Tregan, J. M., J. L. Amestoy, M. Bati, J.-J. Bezian, S. Blanco, L. Brunel, C. Caliot, J. Charon, J.-F. Cornet, C. Coustet, L. d'Alençon, J. Dauchet, S. Dutour, S. Eibner, M. E. Hafi, V. Eymet, O. Farges, V. Forest, R. Fournier, M. Galtier, V. Gattepaille, J. Gautrais, Z. He, F. Hourdin, L. Ibarrart, J.-L. Joly, P. Lapeyre, P. Lavieille, M.-H. Lecureux, J. Lluc, M. Miscevic, N. Mourtaday, Y. Nyffenegger-Péré, L. Pelissier, L. Penazzi, B. Piaud, C. Rodrigues-Viguier, G. Roques, M. Roger, T. Saez, G. Terrée, N. Villefranque, T. Vourc'h, and D. Yaacoub, 2023 : Coupling radiative, conductive and convective heat-transfers in a single Monte Carlo algorithm : A general theoretical framework for linear situations, *PLOS ONE*, **18**, e0283681, publisher : Public Library of Science.

van Zanten, M., B. Stevens, L. Nuijens, A. Siebesma, A. Ackerman, F. Burnet, A. Cheng, F. Couvreux, H. Jiang, M. Khairoutdinov, Y. Kogan, D. Lewellen, D. Mechem, K. Nakamura, A. Noda, B. Shipway, J. Slawinska, S. Wang, and A. Wyszogrodzki, 2011 : Controls on precipitation and cloudiness in simulations of trade-wind cumulus as observed during RICO, *Journal of Advances in Modeling Earth Systems*, **3**.

Villefranque, N., F. Hourdin, L. d'Alençon, S. Blanco, O. Boucher, C. Caliot, C. Coustet, J. Dauchet, M. El Hafi, V. Eymet, O. Farges, V. Forest, R. Fournier, J. Gautrais, V. Masson, B. Piaud, and R. Schoetter, 2022 : The "teapot in a city" : A paradigm shift in urban climate modeling., *Science advances*, **8**, eabp8934.

Watanabe, M., S. Emori, M. Satoh, and H. Miura, 2009 : A PDF-based hybrid prognostic cloud scheme for general circulation models, *Climate Dynamics*, **33**, 795–816, aDS Bibcode : 2009ClDy...33..795W.

Williamson, D., M. Goldstein, L. Allison, A. Blaker, P. Challenor, L. Jackson, and K. Yamazaki, 2013 : History matching for exploring and reducing climate model parameter space using observations and a large perturbed physics ensemble, *Climate Dynamics*, **41**, 1703–1729.

Williamson, D., A. T. Blaker, C. Hampton, and J. Salter, 2015 : Identifying and removing structural biases in climate models with history matching, *Climate Dynamics*, **45**, 1299–1324, number : 5.

Yamada, T., 1983 : Simulations of Nocturnal Drainage Flows by a q2l Turbulence Closure Model, *Journal of the Atmospheric Sciences*, **40**, 91–106, publisher : American Meteorological Society Section : Journal of the Atmospheric Sciences.

Zelinka, M. D., D. A. Randall, M. J. Webb, and S. A. Klein, 2017 : Clearing clouds of uncertainty, *Nature Climate Change*, **7**, 674–678, publisher : Nature Publishing Group.

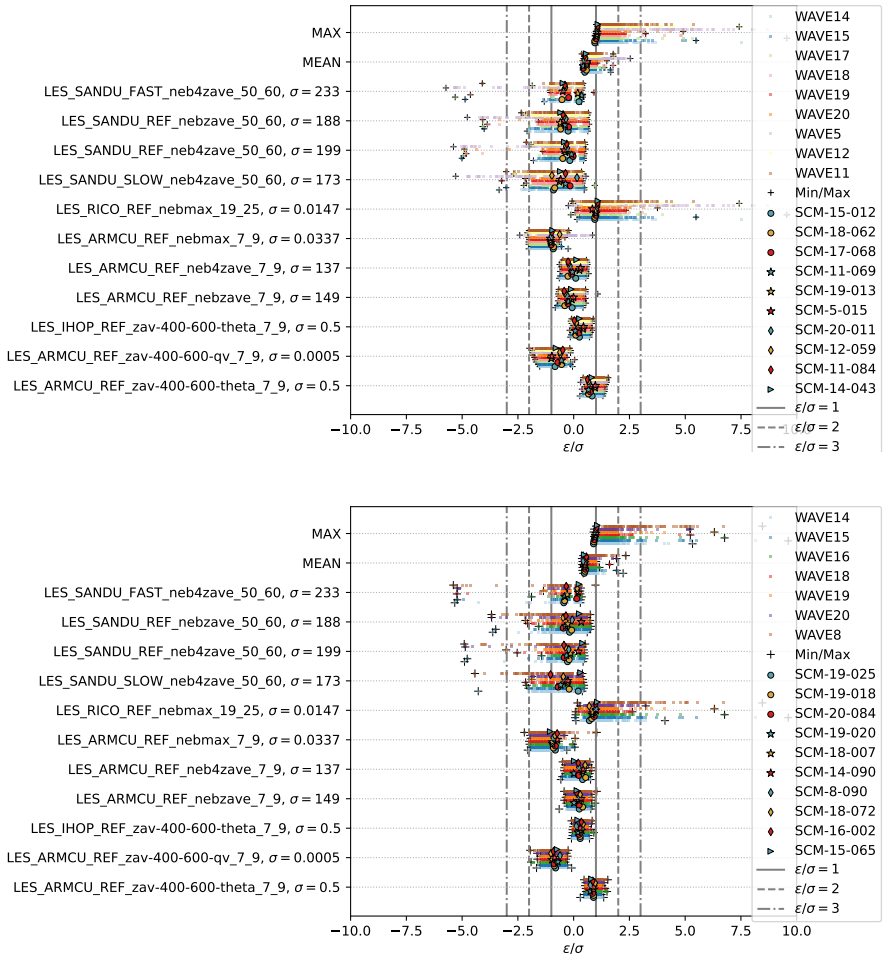

FIGURE 3 – Metric scores over chosen waves including the best simulations. Top : with the previous diagnostic model. Bottom : with the prognostic model. All the scores from the 5 wave simulations are represented with their minimum and maximum scores. The ten best tuning simulations with their scores are highlighted. The 11 metrics are recalled on the left side with their acceptable margins of error σ.

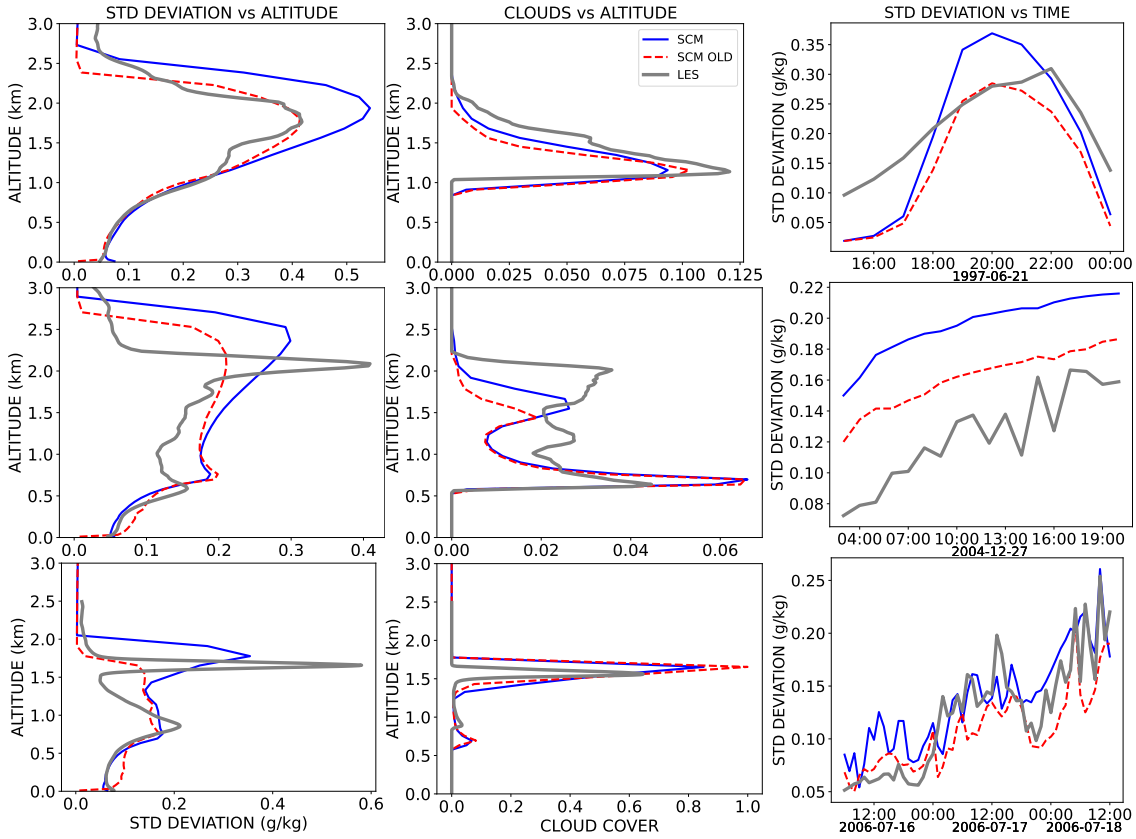

FIGURE 4 – Variance of total specific humidity, including the contribution of thermals from the Bigaussian model, in the cases ARMCU/REF (top), RICO/REF (middle) and SANDU/REF (bottom). Thick gray is the LES, blue is the LMDZ simulation with new prognostic variance and dashed red with previous diagnostic model. On the left the profiles at 7 p.m. for ARMCU, 8 p.m. for RICO and midnight on the last day for SANDU, in the middle the cloud cover profile at the same dates and on the right side temporal evolutions of the averaged variance between 500m and 2500m for ARMCU and RICO and 400m and 2200m for SANDU. These data were obtained with the best tuning simulations for each model.

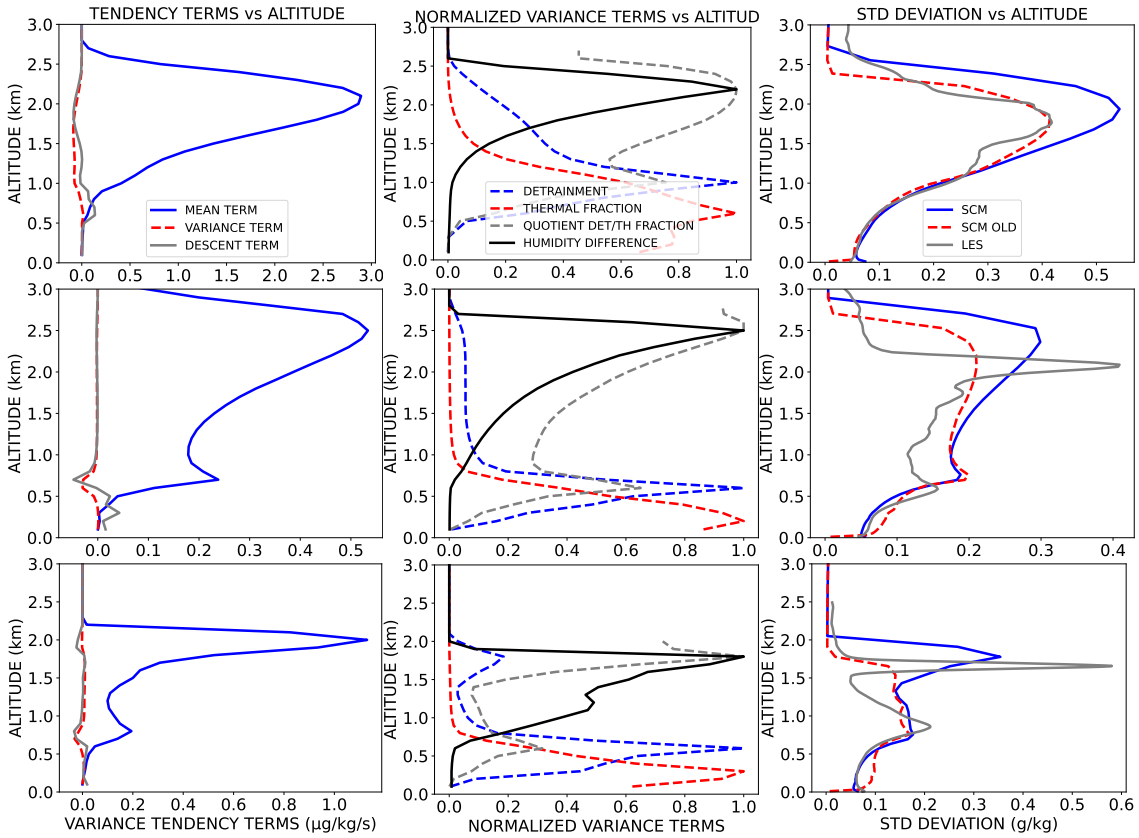

FIGURE 5 – Various profiles in the ARMCU/REF (top) RICO/REF (middle) and SANDU/REF (bottom) cases. On the left : comparison between the 3 source terms of variance in equation 40, blue being $\frac{d}{\rho}(\overline{q_{th}} - \bar{q})^2$ the squared mean difference term, dashed red the variance difference term $\frac{d}{\rho}(\overline{q_{th}^{'2}} - \overline{q^{'2}})$ and gray the subsidence term $\frac{f}{\rho}\frac{\partial \overline{q^{'2}}}{\partial z}$. In the middle the normalized profiles of some physical quantites involved in the variance model : the detrainment rate d (dashed blue), the thermal fraction multiplicative term in the diagnostic model $\frac{\alpha^{\gamma_1}}{1-\alpha}$(dashed red) and the square of the total humidity difference between thermal and environment $(\bar{q}_{th} - \bar{q}_{env})^2$(black). The quotient of the detrainement term by the termal fraction term is also represented (dashed gray). On the right the total humidity variance profiles are remained : blue for the prognostic variance model, dashed red for the diagnostic one and thick gray for the LES. This profiles were computed at the same dates than before.

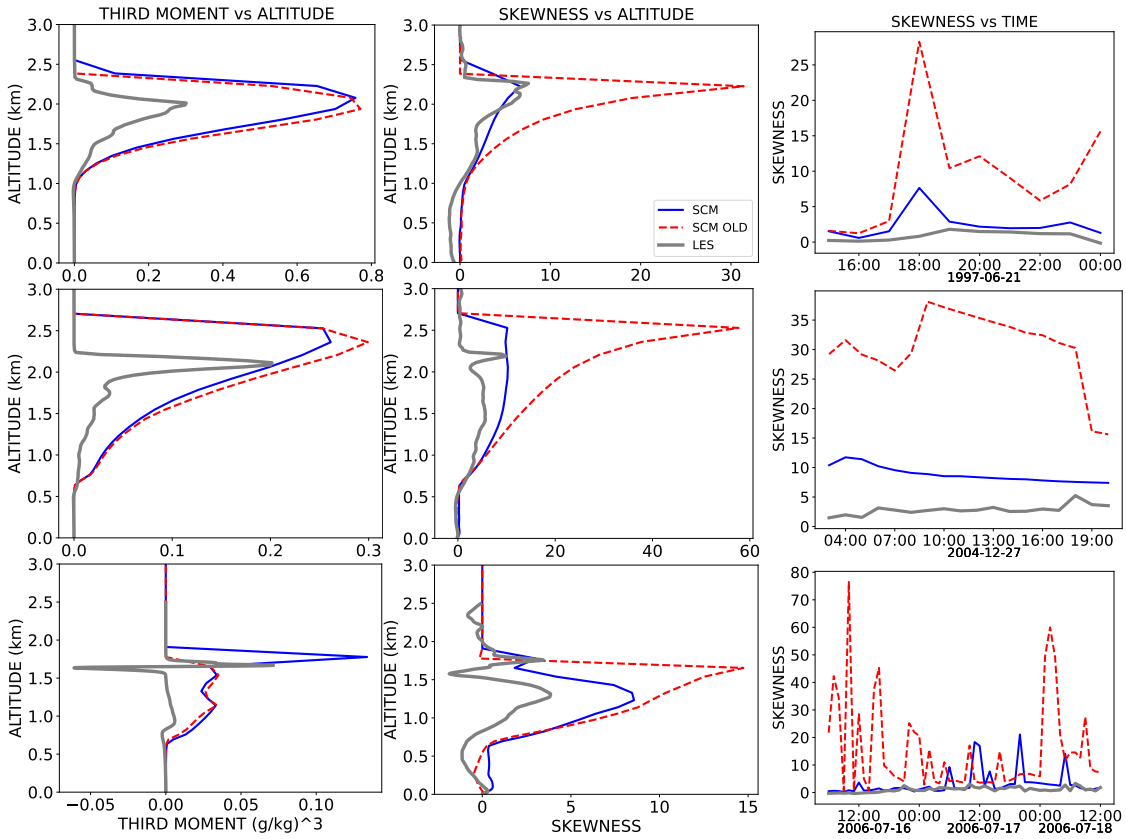

FIGURE 6 – Skewness (centered third order moment (numerator of equation 3) of the saturation deficit distribution on the left, skewness of the saturation deficit distribution and its evolution in time (averaged over the same vertical interval) on the middle and right side. Top ARMCU/REF, middle RICO/REF and bottom SANDU/REF at the same date than previously for left and middle. Blue : SCM with prognostic variance, dshed red : SCM with diagnostic variance, thick gray : LES.

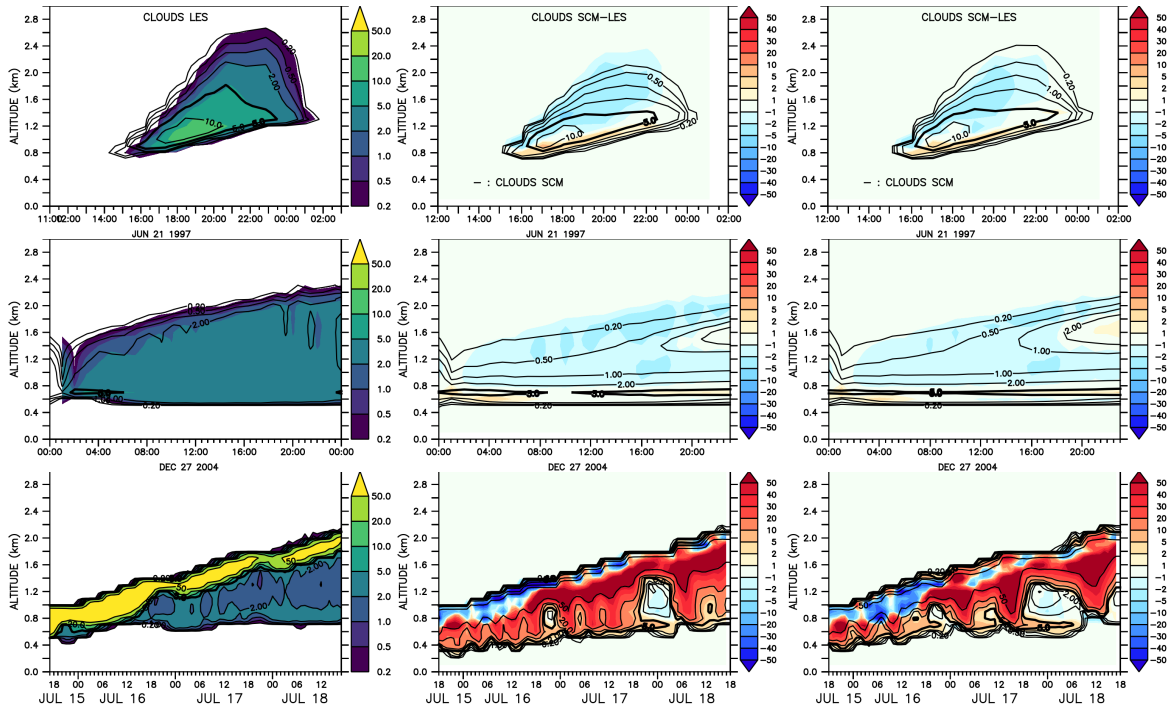

FIGURE 7 – Total cloud cover in the ARMCU/REF (top), RICO/REF (middle) and SANDU/REF (bottom) cases. On the left the LES simulation. In the middle the difference in cloud cover between the best tuning simulation with the old diagnostic model and the LES, black contours indicating the cloud cover in the SCM simulation. On the right the difference in cloud cover between the best tuning simulation with the new prognostic model and the LES, black contours indicating the cloud cover in the SCM simulation.